

Article

Multi-Objective Optimization Design of Cycloid-Pin Gears Based on RV Reducer Precision Transmission Performance

Yunda Zhao, Zhenhua Han *, Qifeng Tan, Wentao Shan, Rirong Li, Hao Wang and Youwu Du

School of Mechanical Engineering, Jiangsu University of Technology, Changzhou 213001, China; 2021655185@smail.jsut.edu.cn (Y.Z.); tqf@jsut.edu.cn (Q.T.); shanwentao520@jsut.edu.cn (W.S.);

2021655267@smail.jsut.edu.cn (R.L.); 2021655244@smail.jsut.edu.cn (H.W.); duyowu@jsut.edu.cn (Y.D.)

* Correspondence: han_jsut@jsut.edu.cn

Abstract: This paper aims to realize multi-objective optimization of cycloid-pin gears to improve the positioning accuracy and load-carrying capacity of the rotary vector (RV) reducer, via the consideration of backlash, transmission error, and torsional stiffness. Initially, the analytical models of the RV transmission backlash and transmission error are developed by using both purely geometrical and equivalent model methods individually. Based on the generalized Hooke's law, a torsion angle model is established to characterize the torsional stiffness of the system, utilizing methods such as Hertzian contact theory and bearing stiffness models. Subsequently, employing the Monte Carlo method, extremum method, and quality loss function, mapping objective functions for dimensional accuracy (tolerance) and transmission performance (backlash, transmission error, and torsional stiffness) are constructed. The geometry dimensions, dimensional accuracy, and modification of the cycloid-pin gear are considered as design variables to create a multi-objective optimization model. The improved Parallel Adaptive Genetic Algorithm using Differential Evolution (PAGA-DE) is used for multi-objective solutions. Through example calculations, the impact of cycloid-pin gear parameters on transmission performance before and after optimization is determined. The reliability of backlash after optimization within $1.5'$ reaches 99.99%, showing an increase of 8.24%. The reliability of transmission error within $1'$ reaches 98.52%, demonstrating an increase of 1.35%. The torsional angle is reduced by 8.9% before optimization. The results indicate that the proposed multi-objective optimization design method for cycloid-pin gears can achieve the goal of improving the transmission performance of the RV reducer.

Keywords: cycloid-pin gear; backlash; transmission error; torsional stiffness; PAGA-DE algorithm



Citation: Zhao, Y.; Han, Z.; Tan, Q.; Shan, W.; Li, R.; Wang, H.; Du, Y. Multi-Objective Optimization Design of Cycloid-Pin Gears Based on RV Reducer Precision Transmission Performance. *Energies* **2024**, *17*, 654. <https://doi.org/10.3390/en17030654>

Academic Editors: Denis N. Sidorov and Fang Liu

Received: 31 December 2023

Revised: 22 January 2024

Accepted: 26 January 2024

Published: 30 January 2024



Copyright: © 2024 by the authors. Licensee MDPI, Basel, Switzerland. This article is an open access article distributed under the terms and conditions of the Creative Commons Attribution (CC BY) license (<https://creativecommons.org/licenses/by/4.0/>).

1. Introduction

The rotary vector (RV) reducer is widely used in high-end precision equipment such as robots, photovoltaic manufacturing and power generation, and semiconductor production, due to its advantages of high energy utilization rate, strong load-bearing capacity, high transmission accuracy, and a wide range of transmission ratios. The cycloid-pin gear is the core transmission component of RV reducers. Its parameter design directly affects the RV reducer ratio, transmission accuracy, load-carrying capacity, and other major transmission properties [1–3]. The design theory and research of cycloid-pin gears are mostly based on traditional mechanical analysis methods. In engineering practice, a tendency towards conservative strength design is often adopted [4,5]. The dimensional accuracy of each component mostly adopts the same tolerance level, which makes the reliability of the RV reducer low, resulting in a waste of human resources. As a result, the design and optimization of the cycloid-pin gear in RV reducers have been a continuous focus of research for scholars both domestically and internationally, aiming to enhance transmission accuracy and carrying capacity and reduce mass loss.

At present, research on the design of cycloid-pin gear primarily focuses on aspects such as error impact analysis, tolerance optimization and selection, profile modification

design, meshing contact analysis and structural dimension parameter analysis. Errors are a critical factor influencing the accuracy of gear transmission, while tolerances determine the machining process requirements for gears [6]. Thus, error impact analysis, tolerance optimization, and selection are focal points of the active design research for cycloid-pin wheel transmission at the microscopic scale. On the basis of analyzing various error factors affecting backlash, Li et al. [7] employed orthogonal experiments and robust design to effectively control the backlash in RV transmissions. Han et al. [8], utilizing the “Sobol” method, established the global sensitivity analysis model of RV reducers to investigate the effects of manufacturing errors, assembly errors, and bearing clearance on transmission accuracy. Li et al. [9], based on the tooth contact analysis, examined the impact of manufacturing errors on the precision of RV transmission. Ahn et al. [10] presented an impact quantitatively analysis of pin radius errors and friction between the cycloid gear and pin on the meshing force in the cycloid-pin gear pair using the FE method. In terms of tolerance optimization and selection, Sun et al. [11] analyzed the sensitivity of various errors in RV reducers and, through Monte Carlo simulations, determined suitable tolerance levels for error parameters. Zhao et al. [12] constructed the distribution model of various errors and tolerances of RV reducers on the basis of the analysis of the backlash model. Chu et al. [13] developed a tolerance selection and assembly method for RV reducers based on a genetic algorithm, aiming to achieve the required backlash precision. Li et al. [14] started with the processing cost of tolerances to achieve tolerance design for the parameters inside the cycloid-pin gear. At the microscopic level, profile modification design is also a pivotal study direction in the design of the cycloid-pin gear. Wan et al. [15] quantitatively analyzed the variations in precision in cycloid-pin gear transmission due to different combinations of profile modifications. Liu et al. [16], starting from the meshing force of the cycloid-pin gear pair, optimized the design of the cycloid gear profile modification. Sun et al. [17] proposed a novel parabolic profile modification method and used a particle swarm algorithm with the minimum transmission error as the optimization objective to obtain the optimum trimming coefficients.

Meshing contact analysis is particularly crucial for the study of gear design [18–20]. Experts have conducted the following research in the field of cycloid-pin gears. Blagojevic et al. [21] conducted a stress analysis of single-stage cycloid gears under working conditions with only one pair of meshing teeth using finite element analysis and experimentally used the strain gauge method for experimental validation. Li et al. [22] established a theoretical contact analysis model of cycloid pin gears considering manufacturing errors and analyzed the effects of tooth shape error and pitch error of cycloid gears on meshing characteristics. Qiao et al. [23] performed transient dynamic analysis on RV reducers to investigate the stress distribution of cycloid-pin gears during the meshing process. Li et al. [24] applied the minimum energy principle to propose a mathematical model for calculating the number of simultaneously meshing teeth in the process of cycloid-pin gear transmission, which was validated by simulation and measurement experiments. Li et al. [25] considered the impact of ring pin position deviation, established an analysis model for the load distribution in the misaligned cycloid-pin gear pair, and analyzed the effects of pin tooth radial position error and phase angle on the meshing characteristics of cycloid-pin gear pair. In addition, scholars conducted qualitative and quantitative analyses of structural dimension parameters at the macro scale. Bednarczyk et al. [26] investigated the effect of the eccentricity of the cycloid gear on meshing force and power loss in gear transmission through optical elastic experiments. A generalized dynamics model of a cycloid-pin gear of an RV reducer considering bearings was developed by Xu et al. [27]. It is used to investigate the effects of geometrical parameters in the cycloid-pin gear pair on the dynamic contact response and internal load transfer characteristics. Zhang et al. [28] analyzed the impact of design parameters of the cycloid-pin gear (eccentricity, radius of pin gear distribution circle, pin gear radius, and width of the cycloid gear, etc.) on the load-bearing capacity from three aspects: load distribution coefficient, torsional stiffness, and contact stress. Li et al. [29] established a calculation model for the meshing stiffness of the cycloid-pin gear pair related

to profile modification and eccentricity errors. They separately explained the effects of profile modification and eccentricity on torsional stiffness, load-bearing transmission error, and contact stress.

The above scholars have analyzed the influence of the design parameters of the cycloid-pin gear more comprehensively. However, the design parameters of components in the cycloid-pin gear transmission system have a relationship of interdependence and mutual influence, and the transmission performance is coupled with each other. Therefore, the design of the cycloid-pin gear of RV reducers should not only comprehensively analyze its failure mode, structural form, and design guidelines, but also make the comprehensive performance of the transmission system to meet the design requirements.

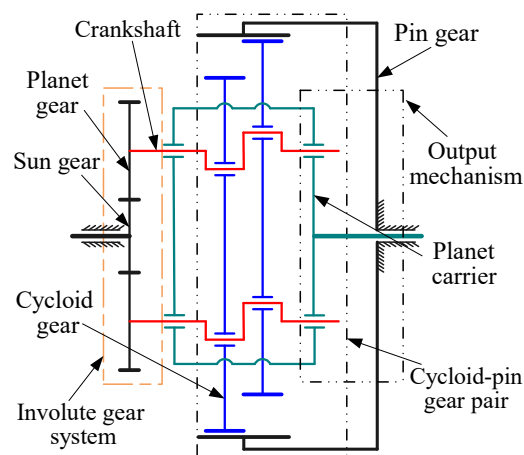
Meanwhile, considering multiple transmission performance indicators for parameter design is a typical multi-objective optimization problem. In this regard, experts have conducted the following research on cycloid-pin gear transmission. Wang et al. [30], with the optimization objectives of achieving the highest transmission efficiency and the smallest volume, considered constraints such as tooth profile, strength, and lifespan. They conducted an optimization design of parameters including the cycloid gear, pin gear, and pin for the cycloid-pin gear transmission. Wang et al. [31] established a multi-objective optimization model with the objectives of the volume of the cycloid-pin gear, the bearing load on the turning arm bearing, and the bending stress on the pin. Zhang et al. [32] optimized the geometric dimensions and modification of RV reducers with the objectives of volume, efficiency, and anti-adhesive capability. Wu et al. [33] proposed an optimization method for the design of the cycloid-pin gear in RV transmissions with transmission error, load of the turning arm bearing, and volume as optimization objectives. The method considers constraints such as tooth profile interference, contact strength, and bearing life. Song et al. [34] proposed a cycloid gear profile design method that considers a composite modification function and transmission error as optimization objectives, determining the magnitude of the profile modification. Furthermore, in the multi-objective optimization of other gear transmission systems, Paridhi et al. [35], considering constraints such as tooth surface contact and bending strength, minimized volume as the optimization objective. They conducted an optimization design for the profile displacement coefficient, number of teeth, face width, and module of helical gears. Daoudi et al. [36], considering constraints such as assembly, bending strength, and tooth surface contact strength, started from the mass, center distance, and efficiency of the epicyclical gear train system. They optimized and improved parameters such as the number of teeth, tooth width, tooth thickness, and shaft diameter. Yao [37] established an optimization model with the objectives of center distance, load factor, and meshing efficiency for spur gear systems. Using the NSGA-II algorithm, they achieved optimization and improvement of design parameters such as module, number of teeth, and transmission ratio. The scholars mentioned above, in the multi-objective optimization of gear transmission, mostly focus on efficiency, volume, and mechanical load-bearing performance, regulating design parameters at the macro scale. Simultaneously, research on related backlash primarily concentrates on error parameter design [7,8] and tolerance allocation issues [11,12]. There is a lack of multi-scale parameter design methods for cycloid-pin gear drives involving comprehensive analysis of backlash and other transmission performance. Moreover, most of the mentioned optimization designs use traditional intelligent optimization algorithms. For different multi-objective optimization models, the computational efficiency and optimization accuracy of the algorithm are quite different.

To address the above issues, this paper proposes a multi-objective optimization design method for cycloid-pin gear pairs, comprehensively considering backlash, transmission error, and torsional stiffness in RV reducers. This method takes the geometric dimensions, dimensional accuracy (tolerance), and modification of cycloid-pin gear pairs as design variables, enabling active regulation of parameters of both macro and micro dual scales on the transmission performance of RV reducers. Additionally, an improved Parallel Adaptive Genetic Algorithm using Differential Evolution (PAGA-DE) is introduced, enhancing

computational efficiency and convergence accuracy during the optimization model-solving process. The research presented in this paper essentially achieves error control in the transmission system and provides guidance for the design of geometric dimensions. The established analytical model offers theoretical support for research and optimization in the field of reducers, while also presenting a novel improvement in the algorithmic domain.

2. Transmission Performance Analysis Model of RV Reducers

In this paper, the standard RV reducer with three crankshafts is the object of study, and its transmission principle is illustrated in Figure 1. The establishment of a reasonable and effective mathematical model for transmission performance, including backlash, transmission error, and torsional stiffness, is the theoretical basis for the analysis and optimization of precision reducer transmission performance. These models are also crucial for achieving the optimal design of the cycloid gears in RV reducers.



Involute gear system includes Sun gear, and Planet gear; Cycloid-pin gear pair includes Crankshaft, Cycloid gear, and Pin gear; Output mechanism includes Planet carrier.

Figure 1. RV reducer transmission schematic.

2.1. Mathematical Model of Backlash in RV Reducers

The root cause of the formation of backlash is gaps between gear meshing pairs (i.e., side clearance) caused by various errors. Errors are generally divided into three main categories: manufacturing errors, assembly errors, and other errors (temperature, force deformation, etc.). Manufacturing errors and assembly errors are important reasons for the generation of geometric return difference. According to the transmission principle, the backlash of the RV reducer primarily comprises three parts: the first-stage involute gear system backlash φ_1 , the second-stage cycloid-pin gear backlash φ_2 , and the backlash in the output mechanism φ_3 . The total backlash φ_Σ of the RV transmission system is obtained by superimposing these three components [11].

$$\varphi_\Sigma = \varphi_1 + \varphi_2 + \varphi_3 \quad (1)$$

2.1.1. Backlash of the Involute Gear System

The primary error parameters considered in calculating the backlash of involute gear systems comprise the average length error E_w of the base tangent, center distance error ΔF_α , and radial runout error ΔF_r of the gear [38]. E_w , ΔF_α , and ΔF_r induce circumferential clearances as illustrated below:

$$\begin{cases} j_{E1} = E_w / \cos \alpha \\ j_{E2} = 2\Delta F_\alpha K_\alpha \tan \alpha \\ j_{E3} = \Delta F_r K_\alpha \tan \alpha \end{cases} , \quad (2)$$

where j_{E1} , j_{E2} and j_{E3} represent the circumferential clearances induced by errors E_w , ΔF_α and ΔF_r , respectively, α is the pressure angle of involute gears, K_α is the conversion factor, $K_\alpha = \sin \alpha' / \sin \alpha$, and α' is the angle of engagement for involute gears.

Converting clearance J_{Ei} into an angle at the output shaft, we can obtain the backlash φ_1 of the involute gear system as follows:

$$\varphi_1 = \frac{180 \times 60 (J_{E1} + J_{E2} + J_{E3})}{i_z \pi r_1}, \quad (3)$$

where i_z is the overall transmission ratio, and r_1 is the radius of the sun gear pitch circle.

2.1.2. Backlash of the Cycloid-Pin Gear Pair

By employing the pure geometric method [39], modification of equidistance Δr_p , moving distance modification ΔR_p , and various errors in the cycloid-pin gear pair are converted into clearances along the meshing, which errors contain the radius of the circle error of the pin gear δR_p , the radius of the pin gear error δr_p , the radial run-out error of the cycloid gear δF_{r1} , the circular position error of the pin gear hole δt , the pitch cumulative error of the cycloid gear δF_p , the radial-moving modification error $\delta \Delta r_p$, the equidistant modification error $\delta \Delta R_p$, and the eccentric error of crankshaft δa . Subsequently, based on the principles of RV transmission and the relationship of motion transmission, these clearances are further transformed into angular displacements at the output shaft, thereby obtaining the backlash of the cycloid-pin gear pair.

$$\varphi_2 = \frac{180 \times 60}{\pi} \left(\frac{\sum \Delta j_{2i}}{az_c} + \Delta \varphi_a \right), \quad (4)$$

where $\sum \Delta j_{2i}$ is the clearance on the meshing line that errors translate into, $\Delta \varphi_a$ is the backlash caused by eccentric error of crankshaft δa , and they can be calculated by

$$\Delta j_{2i} = C_O E_R, \quad (5)$$

where C_O is the coefficient matrix, E_R is the error matrix,

$$\begin{cases} C_O = \text{diag} \left(2, -2\sqrt{1 - K_1^2}, 2\sqrt{1 - K_1^2}, -2, 1/2, 2K_1, -K_1, 2, -2\sqrt{1 - K_1^2} \right) \\ E_R = (\Delta r_p, \Delta R_p, \delta R_p, \delta r_p, \delta F_{r1}, \delta t, \delta F_p, \delta \Delta r_p, \delta \Delta R_p)^T \end{cases},$$

where K_1 is the short width coefficient, a is eccentricity, z_c is the number of teeth of the cycloid gear.

$$\Delta \varphi_a = -2k_n \delta a, \quad (6)$$

where k_n is the conversion coefficient of eccentricity error, and it is expressed as:

$$k_n = \frac{\Delta r_p}{a^2 z_c} - \left(\frac{z_c}{a R_p^2 \sqrt{1 - K_1^2}} + \frac{\sqrt{1 - K_1^2}}{a^2 z_c} \right) \Delta R_p,$$

where R_p is the radius of pin position.

2.1.3. Backlash of the Output Mechanism

The backlash φ_3 generated by the output mechanism is mainly caused by the radial clearance of the turning arm bearing Δu , which is calculated as follows:

$$\varphi_3 = \frac{180 \times 60}{\pi a_0} \Delta u, \quad (7)$$

where a_0 is the center distance of involute planet gear transmission.

2.2. Mathematical Model of Transmission Errors in RV Reducers

This paper adopts the equivalent model method [40] to model and analyze transmission errors in RV reducers. The modeling principle is based on the meshing line analysis method, considering the influence of the phase angles of errors. It projects errors onto the meshing line, transforming them into equivalent meshing errors, and then calculates transmission errors. The overall transmission error calculation for RV reducers includes three parts: first-stage involute gear system transmission error β_1 , second-stage cycloid-pin gear pair transmission error β_2 , and output mechanism transmission error β_3 [33].

$$\beta_{\Sigma} = \beta_1 + \beta_2 + \beta_3 \tag{8}$$

2.2.1. Transmission Error of the Involute Gear System

The errors primarily studied in the involute gear system include the manufacturing eccentricity error of the sun gear E_s , the manufacturing eccentricity error of the planet gear E_{pi} , and the installation eccentricity error of the sun gear A_s . Their relative positions in the gear system are illustrated in Figure 2. In the figure, the center O of the sun wheel is taken as the origin of the coordinate system, a fixed coordinate system XOY is established, and the direction of the meshing line away from the sun gear teeth is set as a positive direction. Using pure geometry, errors E_s , E_{pi} and A_s are projected onto the meshing line, obtaining equivalent meshing errors e_s , e_{pi} and α_s along the meshing line, respectively.

$$\begin{cases} e_s = E_s \cos(\theta_s + \beta_s - A_n) \\ e_{pi} = E_{pi} \cos(\theta_p + \beta_{pi} - A_n) \\ \alpha_s = A_s \cos \gamma_s \cos A_n + A_s \sin \gamma_s \sin A_n \end{cases}, \tag{9}$$

where θ_s is the rotation angle of the sun gear, β_s is the phase angle of the manufacturing eccentricity error of the sun gear, A_n is the angle between the meshing line and the X-axis, $A_n = \theta_c - \alpha' + \alpha_{xi} + 0.5\pi$, θ_c is the angle of the planet carrier, $\theta_c = \theta_s/i_z$, α_{xi} is the relative position of the center of the planet gear in coordinate system XOY , $\alpha_{xi} = 120(i - 1)$ (i represents the i -th planet gear, $i = 1, 2, 3$), θ_p is the rotation angle of the planet gear, $\theta_p = \theta_s[1/i_z + (1 - 1/i_z)z_1/z_2]$, z_1 is the number of teeth of the sun gear, z_2 is the number of teeth of the planet gear, β_{pi} is the phase angle of the manufacturing eccentricity error of the planet gear, and γ_s is the phase angle of the installation eccentricity error of the sun gear.

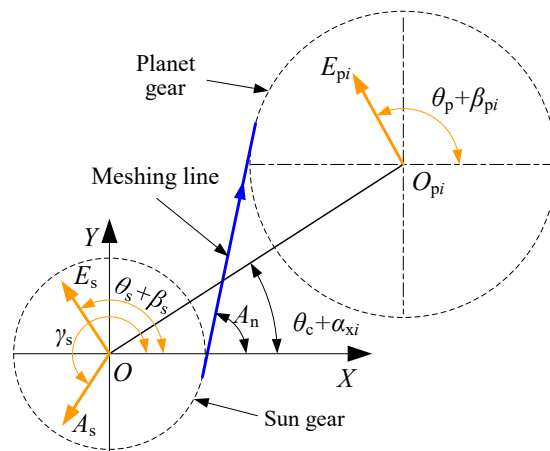


Figure 2. Schematic diagram of involute gear train transmission.

The equivalent meshing errors calculated from Equation (9) are linearly superimposed and transformed into the angular error of the output shaft, representing the transmission error of the involute gear system β_1 :

$$\beta_1 = \frac{180 \times 3600(e_s + e_{pi} + \alpha_s)}{r_1 i_z \pi} \tag{10}$$

2.2.2. Transmission Error of the Cycloid-Pin Gear Pair

The impact of various errors in the cycloid-pin gear pair is directly reflected at the output, exerting a significant influence on the overall transmission error. Therefore, starting from the installation fit and transmission motion relationship between the cycloid gear, pin, and crankshaft, an analysis is conducted on the influence of various error parameters on the system of transmission error [41,42].

Figure 3 depicts the relative positions of errors at a specific moment during the transmission process between the cycloid gear and the pin. In the figure, a Cartesian coordinate system, $X_z O_z Y_z$, whose origin is the center of the pin gear O_z , is employed to represent the reference coordinate system. O_{cj} is the center of the cycloid gear, O_{ak} is the center of the pin, and P is the node where the cycloid gear engages with the pin gear. Based on the meshing line analysis method, the radius of the circle error of the pin gear δR_p , the pitch error of the pin gear δR_a , the radial run-out error of the cycloid gear δF_{r1} , the pitch cumulative error of the cycloid gear δF_p , the radius of the pin gear error δr_p and the clearance error of pin and pin slot δ_H are converted to the equivalent meshing errors $e_R, e_a, e_{Fr}, e_{Fp}, e_r$ and e_H on the meshing line as:

$$\begin{cases} e_R = \delta R_p \cos(\phi_{jk1} - \alpha_{jk}) \\ e_a = \delta R_a \sin(\alpha_{jk} - \phi_{jk1}) \\ e_{Fr} = \delta F_{r1} \cos(\phi_{jk2} - \alpha_{jk}) \\ e_{Fp} = \delta F_p \sin(\alpha_{jk} - \phi_{jk2}) \\ e_r = -\delta r_p \\ e_H = \delta_H \end{cases}, \tag{11}$$

where ϕ_{kj1} is the angle between the line segment $O_z O_{ak}$ and the positive direction of η_j axis, ϕ_{kj2} is the angle between the line segment $O_{cj} O_{ak}$ and the positive direction of η_j axis, and α_{jk} is the angle between the meshing line and the positive direction of the η_j axis.

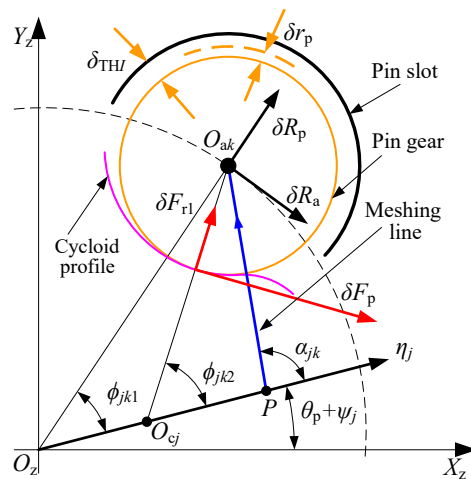


Figure 3. Schematic illustration of errors in cycloid-pin gear pair.

In addition, the change of cycloid gear tooth profile caused by modification is shown in Figure 4. Meanwhile, the coordinate system $X_zO_zY_z$ in the figure is the same as the reference coordinate system in Figure 3. Therefore, the equivalent meshing errors e_{rp} and e_{Rp} of the modification of equidistance Δr_p and the moving distance modification ΔR_p are expressed as:

$$\begin{cases} e_{rp} = \Delta r_p \\ e_{Rp} = -\Delta R_p \left(1 - K_1 \cos \phi_{jk1}\right) \left(1 + K_1^2 - 2K_1 \cos \phi_{jk1}\right)^{-1/2} \end{cases} \quad (12)$$

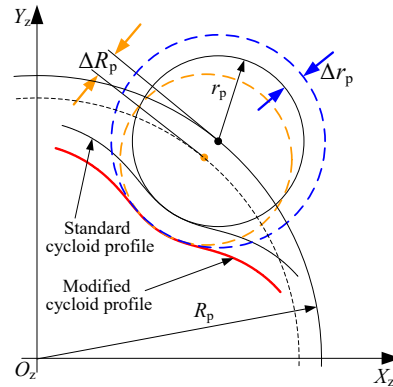


Figure 4. Schematic diagram of cycloid profile modification.

About the installation fit between the cycloid gear and the crankshaft, the existing errors are depicted in Figure 5. The coordinate system $X_zO_zY_z$ represents the pin gear coordinate system, and O_{qi} is the center of the crankshaft hole on the cycloid gear (also the center of the eccentric axis on the crankshaft). Combining with Figure 3, similarly, the expression for transforming the position error of the crankshaft hole on the cycloid gear δC_h and the eccentricity error of the crankshaft δC_s into equivalent meshing errors e_{Ch} and e_{Cs} along the meshing line is:

$$\begin{cases} e_{Ch} = \delta C_h \cos(\theta_c + \alpha_{xi} + \beta_{hji}) \cos(\alpha_{jk} + \theta_p + \psi_j) + \delta C_h \sin(\theta_c + \alpha_{xi} + \beta_{hji}) \sin(\alpha_{jk} + \theta_p + \psi_j) \\ e_{Cs} = \delta C_s \cos(\theta_p + \psi_j + \beta_{sji}) \cos(\alpha_{jk} + \theta_p + \psi_j) + \delta C_s \sin(\theta_p + \psi_j + \beta_{sji}) \sin(\alpha_{jk} + \theta_p + \psi_j) \end{cases}, \quad (13)$$

where β_{hji} and β_{sji} are the phase angle of the errors δC_h and δC_s , respectively, and ψ_j is the relative position of the center of the cycloid gear, $\psi_j = (j - 1)\pi$ (j represents the j -th cycloid gear, $j = 1, 2$).

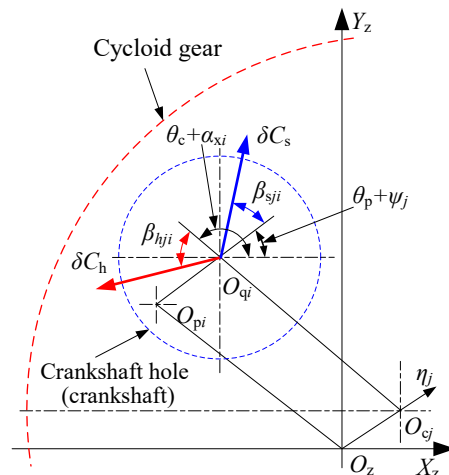


Figure 5. Schematic diagram of the error in the mounting fit of the balance wheel and crankshaft.

The equivalent meshing errors obtained from Equations (11)–(13) are linearly superimposed and converted into angular errors on the output shaft, thus obtaining the transmission error of the cycloid-pin gear pair β_2 .

$$\beta_2 = \frac{180 \times 3600}{\pi} \left[\frac{(e_R + e_a + e_{Fr} + e_{Fp} + e_r + e_H + e_{rp} + e_{Rp} + e_{Ch})}{r'_c} + \frac{e_{Cs}}{r'_c i'_h} \right], \quad (14)$$

where r'_c is the pitch circle radius of the cycloid gear, $r'_c = az_c$, i'_h is the transmission ratio from the crankshaft to the output shaft, $i'_h = \text{abs}(i_h) = \text{abs}(-z_c) = z_c$.

2.2.3. Transmission Error of the Output Mechanism

In the installation fit and transmission motion between the planet carrier and the crankshaft, there is mainly the eccentricity error of the crankshaft hole on the planet carrier δP_q and the installation eccentricity error of the planet carrier δP_a , as shown in Figure 6. With the center of the planet carrier O_s as the coordinate origin, a reference coordinate system $X_s O_s Y_s$ is established, which coincides with the coordinate system $X_z O_z Y_z$ in Figure 3. Based on the principle of equivalent meshing error transformation, the equivalent meshing errors e_{pq} and e_{pa} of errors δP_q and δP_a , on the meshing line can be calculated by

$$\begin{cases} e_{pq} = \delta P_q \cos(\theta_c + \alpha_{xi} + \beta_{ci}) \cos(\alpha_{jk} + \theta_p + \psi_j) + \delta P_q \sin(\theta_c + \alpha_{xi} + \beta_{ci}) \sin(\alpha_{jk} + \theta_p + \psi_j) \\ e_{pa} = \delta P_a \cos \gamma_c \cos(\alpha_{jk} + \theta_p + \psi_j) + A_c \sin \gamma_c \sin(\alpha_{jk} + \theta_p + \psi_j) \end{cases}, \quad (15)$$

where β_{ci} and γ_c are the phase angle of errors δP_q and δP_a , respectively.

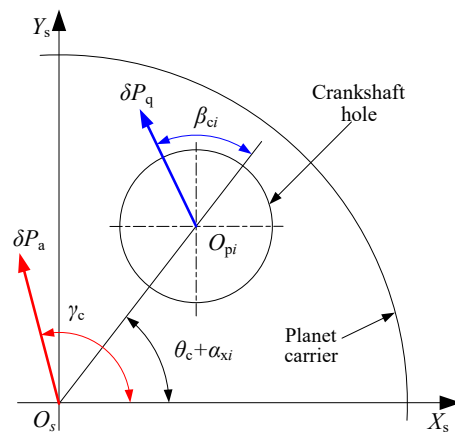


Figure 6. Schematic diagram of errors in the planet carrier.

As above, according to Equation (15), the transmission error β_3 of the output mechanism is given by

$$\beta_3 = \frac{180 \times 3600(e_{pq} + e_{pa})}{\pi r'_c} \quad (16)$$

2.3. Mathematical Model of Torsion Angle in RV Reducers

According to generalized Hooke’s law, under the assumption of constant torque, the torsional angle is inversely proportional to the torsional stiffness under a certain torque. Therefore, a mathematical model of torsional angle is established to characterize the torsional stiffness. According to the RV transmission principle, the overall torsion angle θ_Σ can be divided into involute gear train torsion angle θ_1 , cycloid-pin gear pair torsion angle θ_2 , turning arm bearing torsion angle θ_3 , crankshaft torsion angle θ_4 and planet carrier torsion angle θ_5 .

$$\theta_\Sigma = \theta_1 + \theta_2 + \theta_3 + \theta_4 + \theta_5 \quad (17)$$

Among them, the torsional angle generated by the elastic deformation of the planet carrier can refer to the mathematical model in reference [43], which will not be explained in detail in this paper.

2.3.1. Torsion Angle of the Involute Gear System

From the ISO 6336 [44], the meshing stiffness of involute gears k_χ is calculated as follows:

$$k_\chi = (0.75\varepsilon + 0.25)C_M C_R C_B B \frac{1}{q}, \tag{18}$$

where ε is the contact degree of gear meshing, C_M is the theoretical correction coefficient, $C_M = 0.8$, C_R is the structure coefficient of the wheel blank, $C_R = 1$, C_B is the basic tooth profile coefficient, $C_B = 1$, B is the tooth width of involute gear, and q is the gear flexibility. Its calculation formula is

$$q = 0.04723 + \frac{0.15551}{z_{n1}} + \frac{0.25791}{z_{n2}} - 0.00635x_1 - 0.11654 \frac{x_1}{z_{n1}} - 0.00193x_2 - 0.24188 \frac{x_2}{z_{n2}} + 0.00529x_1^2 + 0.00182x_2^2, \tag{19}$$

where z_{n1} is the equivalent number of teeth of the solar wheel, z_{n2} is the equivalent number of teeth of the planet gear (when the gear is straight teeth, $z_{n1} = z_1$, $z_{n2} = z_2$), x_1 is the displacement coefficient of the solar wheel, and x_2 is the displacement coefficient of the planet gear.

Based on Hooke’s law and combined with Equation (18), the linear deformation $\Delta\delta_p$ of involute gear transmission is represented as

$$\Delta\delta_p = \frac{F_t / \cos \alpha'}{k_\chi}, \tag{20}$$

where F_t is the tangential component of involute gear.

The linear deformation $\Delta\delta_p$ is converted to the sun gear angle, which is reduced by the transmission ratio i_z to obtain the torsion angle θ_1 of the involute gear system in the output shaft.

$$\theta_1 = \frac{180 \times 3600 \Delta\delta_p \cos \alpha'}{\pi r_1 i_z} = \frac{180 \times 3600 F_t}{\pi k_\chi r_1 i_z} \tag{21}$$

2.3.2. Torsion Angle of the Cycloid-Pin Gear Pair

There is only one pair of teeth engaged in theory when the cycloid gear is engaged with the pin gear after modification. The other pairs of teeth have different sizes of initial meshing clearance $\Delta_1(\varphi_k)$ [45]. At the same time, δR_p and δr_p also produce a small gap $\Delta_2(\varphi_k)$, which affects the size of the clearance $\Delta_1(\varphi_k)$. Therefore, the initial meshing clearance $\Delta(\varphi_k)$ becomes

$$\begin{cases} \Delta(\varphi_k) = \Delta_1(\varphi_k) - \Delta_2(\varphi_k) \\ \Delta_1(\varphi_k) = \Delta r_p \left(1 - S^{-1/2} \sin \varphi_k\right) - \Delta R_p \left(1 - K'_1 \cos \varphi_k - \sqrt{1 - K'^2_1} \sin \varphi_k\right) S^{-1/2} \\ \Delta_2(\varphi_k) = \delta r_p \left(1 - S^{-1/2} \sin \varphi_k\right) + \delta R_p \left(1 - K'_1 \cos \varphi_k - \sqrt{1 - K'^2_1} \sin \varphi_k\right) S^{-1/2} \end{cases}, \tag{22}$$

where $S = 1 + K'^2_1 - 2K'_1 \cos \varphi_k$, ($k = 1, 2, \dots, z_p/2$), $K'_1 = az_p / (R_p + \Delta R_p)$.

Under the action of the load torque T_c , the cycloid gear contacts deformation produced with the pin, causing the cycloid gear to rotate by a small angle β_c . According to the deformation coordination principle, the normal deformation $\Delta\delta_k$ of each tooth on the cycloid gear is given by

$$\Delta\delta_k = l_k \beta_c = \frac{l_k \Delta\delta_{\max}}{r'_c}, \tag{23}$$

where l_k is the distance from the common normal of the engagement point of the k -th pin tooth or the normal of the point to be engaged to the center of the cycloid gear, $l_k = r'_c S^{-1/2} \sin \varphi_k$, $\Delta\delta_{\max}$ is the maximum contact deformation.

Based on the Hertzian contact theory [25], the contact deformation w of the cycloid gear with the pin is

$$w = \frac{2F}{\pi b_1} \left[\frac{1 - \mu_1^2}{E_1} \left(\frac{1}{3} + \ln \frac{4R_1}{L} \right) + \frac{1 - \mu_2^2}{E_2} \left(\frac{1}{3} + \ln \frac{4R_2}{L} \right) \right], \quad (24)$$

where F is the force exerted on the two cylinders, b_1 is the contact length of the two cylinders, μ_1 and μ_2 are the Poisson's ratios of the two cylinders, respectively, E_1 and E_2 are the modulus of elasticity of the two cylinders, respectively, R_1 and R_2 are the radii of the two cylinders, in addition to this

$$L = 1.60 \sqrt{\frac{F}{b} K_D \left(\frac{1 - \mu_1^2}{E_1} + \frac{1 - \mu_2^2}{E_2} \right)}, \quad (25)$$

where when the cylinder is convex contact with the cylinder, $K_D = 2R_1R_2/(R_1 + R_2)$, and when the cylindrical and cylindrical holes are convex and concave contact, $K_D = 2R_1R_2/(R_1 - R_2)$.

If $F = F_{\max}$, combined with Equation (24), the maximum deformation $\Delta\delta_{\max}$ can be obtained.

$$\Delta\delta_{\max} = w_{\max} \quad (26)$$

If the normal displacement $\Delta\delta_k$ of a tooth pair is greater than the meshing clearance $\Delta(\varphi_k)$, the pair of teeth is correspondingly in load-bearing mesh. The meshing force F_k of the meshing tooth pair of the cycloid-pin gear is

$$F_k = \frac{\Delta\delta_k - \Delta(\varphi_k)}{\Delta\delta_{\max}} F_{\max} \quad (27)$$

According to the torque equilibrium condition, we obtain $T_c = \sum_{k=g}^G F_k l_k$ (g is the starting tooth number, G is the end meshing tooth number). Then, combining with Equation (27), the maximum meshing force F_{\max} can be deduced as

$$F_{\max} = \frac{T_c}{\sum_{i=b}^e \left(\frac{l_i}{r'_c} - \frac{\Delta(\varphi_i)}{\Delta\delta_{\max}} \right) l_i} \quad (28)$$

In light of the deformation coordination condition Equation (23) and torque balance Equation (28), the mechanical analysis model of a cycloid-pin gear is founded. The calculation flow is as follows:

Step 1, the maximum meshing force is proposed as $F_{\max0}$, that is substituted into Equation (24) to calculate the maximum deformation $\Delta\delta_{\max0}$. $\Delta\delta_{\max0}$ is substituted into Equation (28) to obtain $F_{\max1}$.

Step 2, the difference judgment, if $|F_{\max1} - F_{\max0}| > 0.1F_{\max1}$, assign the $F_{\max1}$ value to $F_{\max0}$, and then repeat the cycle step 1.

Step 3, when $|F_{\max1} - F_{\max0}| < 0.1F_{\max1}$ is stopped, the maximum meshing force is $F_{\max} = (F_{\max0} + F_{\max1})/2$, and the meshing interval $[g, G]$ and the maximum deformation $\Delta\delta_{\max}$ can be obtained from Equations (22)–(26).

From the maximum deformation $\Delta\delta_{\max}$, the cycloid gear angle $\Delta\theta_b$ caused by contact deformation is

$$\Delta\theta_b = \frac{\Delta\delta_{\max}}{R_{p1}}, \quad (29)$$

where R_{p1} is the pitch circle radius of the pin gear, $R_{p1} = az_p$.

By converting the cycloid gear angle $\Delta\theta_b$ to the output shaft, the cycloid-pin gear pair torsion angle θ_2 can be obtained.

$$\theta_2 = \frac{180 \times 3600}{\pi} \Delta\theta_b i_b, \tag{30}$$

where i_b is the transmission ratio of the output shaft relative to the pinwheel when the involute sun gear is fixed, $i_b = -(1 - i_z)/i_z$.

In order to analyze the torsional stiffness of cycloid-pin gear pair, the equivalent torsional stiffness mathematical model was established based on the above mechanical analysis model. Using Hertz theory, considering the distribution radius error δR_p and the radius error δr_p , the meshing stiffness k_b of cycloid gear and pinwheel single pair teeth [46] is

$$k_b = \begin{cases} \frac{\pi b E R'_p S^{3/2}}{4(1-\mu^2)(R'_p S^{3/2} + 2T'r'_p)}, & (\rho_2 > 0) \\ \frac{\pi b E}{4(1-\mu^2)}, & (\rho_2 \leq 0) \end{cases}, \tag{31}$$

where b is the width of cycloid gear teeth, μ is the Poisson ratio, $\mu = 0.3$, E is the elasticity modulus, $E = 2.06 \times 10^{11}$ Pa, $R'_p = R_p + \delta R_p$, $S = 1 + K_1'^2 - 2K_1' \cos \varphi_k$, φ_k is the angle of the k -th pin tooth to the swivel arm $O_c O_z$, $r'_p = r_p + \delta r_p$, ρ_2 is the actual radius of curvature of the cycloid gear, $T' = K_1'(z_p + 1) \cos \varphi_i - (1 + z_p K_1'^2)$.

Based on Equation (31), the equivalent torsional stiffness k_k of a single pair of teeth can be calculated as

$$k_k = k_b l_k^2 \tag{32}$$

The torsional stiffness K of the cycloid-pin gear pair is obtained by linear superposition of equivalent torsional stiffness k_k of the contact tooth pair at different phase angles.

$$K = \sum_{k=g}^G k_k \tag{33}$$

2.3.3. Torsion Angle of the Turning Arm Bearing

Take a rotor bearing in a cycloid gear as an example. Its force is shown in Figure 7. In the figure, $X_z O_z Y_z$ represents the global coordinate system established on the pinwheel, and $X_q O_q Y_q$ is the local coordinate system of the turning arm bearing.

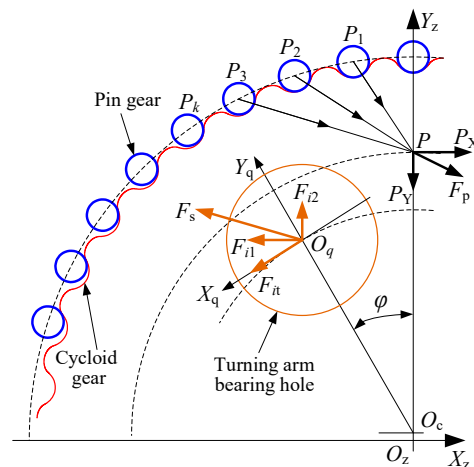


Figure 7. Force analysis diagram of turning arm bearing.

The meshing force of the contact tooth pair of cycloid-pin gear pair moves along the meshing line to node P . The combined force is F_p and is decomposed into the component forces P_X and P_Y along the X_z axis and Y_z axis [47].

$$\begin{cases} P_X = \sum P_x = \frac{M_a}{2r_c} = \frac{M_a z_p}{2K'_1 R'_p z_c} \\ P_Y = K_y P_X \\ K_y = \frac{2}{\pi} \left(\frac{1}{K'_1} + \frac{K'_1{}^2 - 1}{2K'_1{}^2} \ln \frac{1+K'_1}{1-K'_1} \right) \end{cases}, \tag{34}$$

where M_a is the load borne by the RV transmission, with its maximum value being 2.5 times the rated torque T .

The force generated by the crankshaft on the cycloid gear can be divided into three parts: F_{it} , F_{i1} and F_{i2} . The equation can be obtained from the moment equilibrium condition, as shown below

$$\begin{cases} P_X r'_c - \sum_{i=1}^{N_q} F_{it} a_0 = 0 \\ P_X - \sum_{i=1}^{N_q} F_{i1} = 0 \\ P_Y - \sum_{i=1}^{N_q} F_{i2} = 0 \end{cases}, \tag{35}$$

where N_q is the number of crankshafts

The component forces F_{it} , F_{i1} and F_{i2} are projected onto the X_q and Y_z axes of the local coordinate system to obtain the component forces F_x and F_y . Thereby, the radial force F_s on the turning arm bearing is formulated as

$$F_s = \sqrt{F_x^2 + F_y^2}, \tag{36}$$

where $F_x = F_{it} + F_{i1} \cos \varphi + F_{i2} \sin \varphi$, $F_y = F_{i1} \sin \varphi + F_{i2} \cos \varphi$, and φ is the angle between the Y_q axis and Y_z axis.

Using the stiffness model of cylindrical roller bearing [48], the stiffness of turning arm bearing k_s is expressed as

$$k_s = 0.34 \times 10^4 F_s^{0.1} N_g^{0.9} L^{0.8} \cos(\theta_j)^{1.9}, \tag{37}$$

where N_g is the number of rollers, L is the effective length of the roller, and θ_j is the contact angle of the rolling element.

According to the stiffness k_s of the turning arm bearing, the relative displacement $\Delta\delta_s$ of the inner and outer rings of the turning arm bearing can be calculated

$$\Delta\delta_s = \frac{F_s}{k_s} \tag{38}$$

The relative displacement $\Delta\delta_s$ is converted into the angle of the output shaft, that is, the torsion angle θ_3 of the turning arm bearing.

$$\theta_3 = \frac{180 \times 3600 z_c \Delta\delta_s i_b}{\pi z_p a_0} \tag{39}$$

2.3.4. Torsion Angle of the Crankshaft

In transmission, the crankshaft is not only subject to the circumferential force distributed by the cycloid gear in the bearing hole of the boom, but also to the torque action, as shown in Figure 8. Therefore, the torsion angle of the crankshaft is caused by both

circumferential bending deformation and torsional deformation of the crankshaft, which will be analyzed separately in the following.

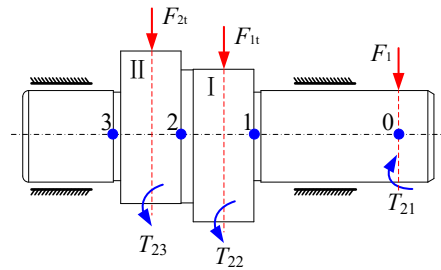


Figure 8. Force analysis diagram of crankshaft.

(1) In the figure, F_{1t} and F_{2t} are separately the circumferential forces of the two cycloid gears on the crank shaft under the action of torque, $F_{1t} = F_{2t} = T/(6a_0)$. F_1 is the force caused by the input torque of the planet gear, $F_1 = T_{in}/(3r_1)$, and T_{in} is the input torque. Section I and section II represent the assumed action sections of two cycloid gears on the crankshaft. According to the beam deflection theory of material mechanics, the deflection of the crankshaft subjected to F_{1t} , F_{2t} and F_1 in section I and section II is calculated, respectively. However, due to the different deflections of the two cross-sections, the average value f_m should be used to calculate the output shaft angle $\Delta\theta_{q1}$ caused by the bending deformation of the crankshaft.

$$\Delta\theta_{q1} = \frac{f_m}{a_0} = \frac{f_I + f_{II}}{2a_0}, \tag{40}$$

where f_I is the deflection at section I, and f_{II} is the deflection at Section II.

(2) According to the elastic deformation theory of material mechanics, the crankshaft will have a relative angle $\Delta\varphi_s$ between Section 0 and Section 3 under the action of torque.

$$\Delta\varphi_s = \sum_{t=1}^3 \frac{T_{2t}l_{2t}}{GJ_{pt}}, \tag{41}$$

where T_{2t} is the torque of each section of the crankshaft, $T_{23} = T_{22} = T_{21}/2$, $T_{21} = Tz_2/(3i_z z_1)$, l_{2t} is the length of each shaft of the crankshaft, G is the shear modulus, $G = 8 \times 10^4 \text{MPa}$, J_{pt} is the polar moment of inertia, $J_{pt} = \pi d_t^4/32$, and d_t is the diameter of each shaft of the crankshaft.

The angle of torsion $\Delta\varphi_s$, generated by the crankshaft under the action of the torque, translates into the angle of rotation $\Delta\theta_{s2}$ of the output shaft as

$$\Delta\theta_{s2} = \frac{\Delta\varphi_s z_2}{z_1 i_z} \tag{42}$$

The total torsion angle θ_4 of the crankshaft is obtained by superimposing the torsion angle obtained by Equations (40) and (42).

$$\theta_4 = \Delta\theta_{s1} + \Delta\theta_{s2} \tag{43}$$

3. Multi-Objective Optimization Model and Optimization Algorithm

3.1. Establishment of Multi-Objective Optimization Model

Figure 9 shows the flow chart for building a multi-objective optimization model for RV reducers. By analyzing the transmission performance of RV reducers in Section 1, the functional relationship between basic parameters (geometrical dimensions, error parameters and modification) and transmission performance has been achieved. Then, the Monte Carlo method, extreme value method, and quality loss function are employed to further analyze the mapping relationship between dimensional accuracy (error parameter tolerance) and backlash, transmission error, and torsional angle (torsional stiffness). Finally, three objective

functions are acquired, representing the maximum backlash characterization coefficient, the minimum mean transmission error, and minimum torsional angle. Simultaneously, design variables and reasonable constraints are selected.

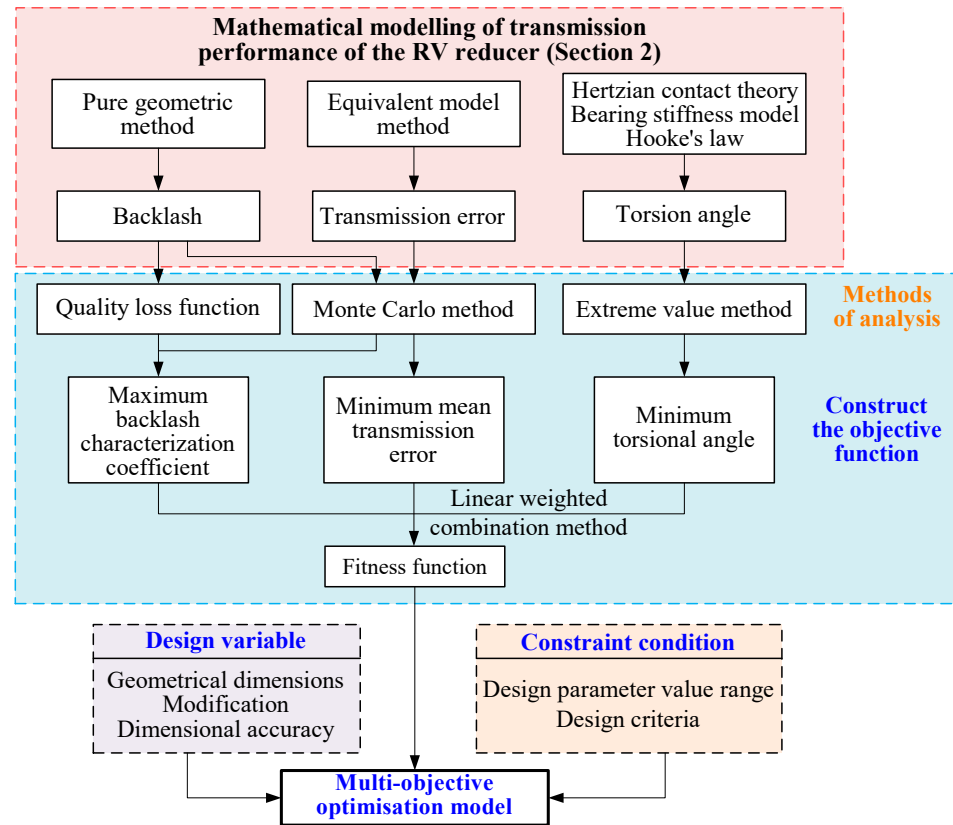


Figure 9. Mathematical model for multi-objective optimization.

3.1.1. Objective Function

(1) Given that the errors are mutually independent and follow certain probability distributions within the tolerances, this paper employs the Monte Carlo method to find the mapping relationship between dimensional accuracy and transmission accuracy. The Monte Carlo experimental simulation N_S is set to 20,000 times. Experimental simulations are conducted based on the backlash mathematical model established in Section 2.1. Using the experimental sample data, the reliability coefficient is calculated by dividing the number $s_1(X)$ of backlashes within $1.5'$ by the total number $S_1(X)$ of simulations.

$$S_1(X) = s_1(X) / N_S \tag{44}$$

The quality loss function $L(T)$ is introduced to take into account both precision requirement and quality cost [49].

$$\begin{cases} L(T_i) = kT_i^2 / 4 \\ C(T_i) = \sum L(T_i) \end{cases} \tag{45}$$

where k is the loss coefficient, $C(T_i)$ is the total quality loss, and T_i is the tolerance value of each error.

By combining the reliability coefficient with the quality loss function, the backlash characterization coefficient is established as the objective function $f_1(X)$, and the formula is as follows:

$$\max f_1(X) = S_1(X) [C(T) / C(T_{\max})], \tag{46}$$

where $C(T_{\max})$ is the maximum quality loss.

(2) The quality cost function of tolerance has been included in the establishment of the backlash objective function, so only the Monte Carlo method is used to establish the transmission error objective function. According to the experimental simulation sample data, the mean transmission error is calculated as the objective function $f_2(X)$, and the formula is as follows:

$$\begin{cases} S_{2i}(X) = \max(\beta_1 + \beta_2 + \beta_3) - \min(\beta_1 + \beta_2 + \beta_3) \\ \min f_2(X) = \left(\sum_i^{N_s} S_{2i}(X) \right) / N_s \end{cases}, \quad (47)$$

where $S_{2i}(X)$ is the transmission error obtained by the simulation of the i experiment.

(3) The extreme value method is used to analyze the error in the mathematical model of torsional angle (torsional stiffness). The principle is to take the maximum value of the error within the tolerance and substitute it into the model. In the case of constant load torque, the torsional angle is inversely proportional to the torsional stiffness. To enhance the load-bearing performance of reducers, the minimum torsional angle objective function $f_3(X)$ is established, expressed as:

$$\min f_3(X) = \theta_1 + \theta_2 + \theta_3 + \theta_4 + \theta_5 \quad (48)$$

(4) In order to make the backlash characterization coefficient, the mean value of transmission error and the torsion angle objective function reach an optimal equilibrium state under the interaction. Based on this, the linear weighted combination method is used to construct the fitness function $F(X)$.

$$\max F(X) = w_1 \frac{f_1(X)}{D_{n1}} + w_2 \frac{D_{n2}}{f_2(X)} + w_3 \frac{D_{n3}}{f_3(X)}, \quad (49)$$

where w_i is the weighting factor, the corresponding weighting factor of each objective function in this paper is $w_1 = 0.33$, $w_2 = 0.33$, $w_3 = 0.34$, and D_{ni} is the dimensionless coefficient. This paper takes the optimal value of each objective function under single-objective optimization ($i = 1, 2, 3$).

3.1.2. Design Variable

As a core component of RV reducers, the design parameters of the cycloid-pin gear pair play a crucial role in the overall transmission performance of the RV system. According to the established mathematical model of backlash, transmission error, and torsion angle, the geometrical dimensions, modification, and dimensional accuracy of cycloid-pin gear pair are selected as the design variables, which are expressed as:

$$X = (R_p, r_p, a, b, \Delta r_p, \Delta R_p, T_{\delta R_p}, T_{\delta r_p}, T_{\delta F_r}, T_{\delta F_p}),$$

where R_p is the radius of pin position, r_p is the radius of pins, a is the eccentricity, b is the width of the cycloid gear, Δr_p is the modification of equidistance, ΔR_p is the moving distance modification, $T_{\delta R_p}$ is the tolerance of the pin distribution radius, $T_{\delta r_p}$ is the tolerance of the pin radius, $T_{\delta F_r}$ is the tolerance of the run-out error of the cycloid gear, and $T_{\delta F_p}$ is the tolerance of the pitch cumulative error of the cycloid gear.

3.1.3. Constraint Condition

The constraint conditions are primarily determined from two aspects: the design parameters and design criteria of the cycloid-pin gear pairs [23,30,33].

Among the design parameters, the short width coefficient K_1 affects the tooth shape of cycloid gears, thereby affecting the load-bearing force of cycloid-pin gear pairs. The pin-diameter coefficient K_2 plays an important role in meeting the strength requirements

of the pin gear housing with the pin and avoiding mutual collision between the pin. The tolerance accuracy $T_{\delta i}$ is the focus of the study of gear transmission accuracy. The width of the cycloid gear b is determined by the diameter of pinwheel central circle D_p . Thus, their constraint ranges are shown in Table 1.

Table 1. Constraints on the structural parameters of the cycloid-pin gear pair.

Serial Number	Parameter	Range of Values			
$g_1(X)$	Number of cycloid gear teeth z_c	≤ 11	13~23	25~59	61~87
	Short width coefficient K_1	0.42~0.55	0.48~0.74	0.65~0.9	0.75~0.9
$g_2(X)$	Number of pins z_p	12~14	24~36	36~60	60~88
	Pin-diameter coefficient K_2	2.8~2	2~1.25	1.6~1	1.5~0.99
$g_3(X)$	Diameter of pinwheel central circle D_p	95~105	106~120	140~160	165~185
$g_4(X)$	Tolerance accuracy $T_{\delta i}$	IT4~IT6			
$g_5(X)$	Width of cycloid gear b	$0.05D_p \sim 0.1D_p$			

Where the range of values of K_1 is related to the number of cycloid gear teeth z_c , $K_1 = az_c/R_p$, the range of values of K_2 is determined by the number of pins z_p , $K_2 = R_p \sin(180/z_p)/r_p$, and D_p ranges from 140 to 160.

In the design of the cycloid-pin gear, to avoid the cycloid gear tooth profile from producing the top cut or sharp angle, it is necessary to make the radius of pins less than the minimum radius of curvature of the cycloid gear cam portion. At the same time, it is also necessary to ensure that meets the requirements of the strength, so add the constraint of contact stress between the pin gear and the cycloid gear. Because of the gear processing, manufacturing errors are inevitable. To facilitate the assembly and disassembly, lubrication and deformation, and other conditions, the cycloid gear and pin need to ensure a certain meshing clearance. Reducer service life is an important issue that cannot be ignored, and the service life of the RV reducer generally depends on the life of the bearings. The transmission efficiency of the RV reducer is also an important performance indicator, so it is necessary to ensure transmission efficiency while improving the transmission accuracy and load-bearing performance. Summarize the detailed expression of the above, shown in Table 2.

Table 2. Constraints on the design criteria for the cycloid-pin gear pair.

Serial Number	Constraint Condition	Calculation Formula for the Range of Values
$g_6(X)$	Avoiding top cutting or sharp angle	$\begin{cases} r_p - (1 + K_1)^2 R_p / (z_p K_1 + 1) < 0, & ((z_p - 2) / (2z_p - 1)) \geq K_1 \\ r_p - R_p \sqrt{27(1 - K_1^2)(z_p - 1)(z_p + 1)^{-3}} < 0, & (1 > K_1 > (z_p - 2) / (2z_p - 1)) \end{cases}$
$g_7(X)$	Contact stress between the pin gear and the cycloid gear	$0.418 \sqrt{\frac{E}{b} \left(\frac{F_i}{\rho_e}\right)_{\max}} - [\sigma_H] \leq 0$
$g_8(X)$	Meshing clearance	$\frac{2(\Delta R_p - \delta R_p)}{az_c} \sqrt{1 - K_1^2} - \frac{2(\Delta r_p - \delta r_p)}{az_c} \leq 0$
$g_9(X)$	Bearing life	$5000 - \frac{10^6}{60n_p} \left(\frac{C}{P}\right)^{\frac{10}{3}} \leq 0$
$g_{10}(X)$	Transmission efficiency	$0.8 - \eta_{12}\eta_S(1 - \eta_M) \leq 0$

In the table, F_i is the engagement force at the contact point of the cycloid-pinwheel, ρ_e is the equivalent radius of curvature, $\rho_e = |\rho_i r_{rp} / (\rho_i - r_{rp})|$, ρ_i is the radius of curvature of the cycloid gear at the engagement point, $[\sigma_H]$ is the allowable contact stress, $[\sigma_H] = 1500$ MPa, n_p is the rotating speed of the boom bearing, $n_p = n_1 [1 + 1 / (z_p - 1)]$, C is the rated dynamic load of the boom bearing, P is the actual dynamic load on the boom bearing, η_S is the total bearing efficiency, $\eta_S = 0.99$, η_M is the hydraulic loss

efficiency, $\eta_M = (0.01 \sim 0.02)\eta_{12}$, η_{12} is the meshing efficiency of RV transmission, and it is expressed as

$$\eta_{12} = \frac{1 - i_1 i_2 (\eta_1 \eta_2)}{i_z}, \quad \eta_1 = 1 - 2.3 f_z \left(\frac{1}{z_1} + \frac{1}{z_2} \right), \quad \eta_2 = \frac{1 - (R_p - r_p) \frac{4 f_z}{K_1 z_c R_p \pi}}{1 + (R_p - r_p) \frac{4 f_z}{K_1 R_p \pi}}$$

where f_z is the friction coefficient of tooth meshing, $i_1 = -z_2/z_1$, $i_2 = z_p/(z_p - z_c)$.

In summary, the multi-objective optimization model established by combining the objective function and constraints can be expressed as

$$\begin{aligned} \max F(X) &= [\max f_1(X), \min f_2(X), \min f_3(X)] \\ \text{s.t.} \quad &\begin{cases} g_{i\min}(X) \leq g_i(X) \leq g_{i\max}(X), & (i = 1, 2, \dots, 5) \\ g_i(X) \leq 0, & (i = 6, 7, \dots, 10) \end{cases} \end{aligned} \tag{50}$$

3.2. PAGA-DE Algorithm

Traditional Genetic Algorithm (GA) [50,51] is commonly used to solve objective optimization models, but it has drawbacks such as a tendency to fall into local optima, poor convergence accuracy, and low computational efficiency for solving complex models. To overcome these shortcomings, an improved Parallel Adaptive Genetic Algorithm using Differential Evolution (PAGA-DE) is proposed. The principle of this algorithm is to integrate the mutation operator from the Differential Evolution (DE) algorithm [52,53] into the crossover operator of the Adaptive Genetic Algorithm (AGA) [54,55], redesign the crossover operator, and utilize parallel operation [56] throughout the algorithm. The improved crossover operator is illustrated in Figure 10. First, it identifies the crossover individual P_i^s in the current iteration population. Second, it randomly selects two individuals P_r^s and P_t^s from the current population and calculates the crossover copy $P_i^{s'}$. Finally, it performs a crossover calculation between P_i^s and $P_i^{s'}$ to obtain the individual for the next iteration P_i^{s+1} , where s is the number of current iterations, $s + 1$ is the number of the next iteration, i is the serial number of cross individuals in the current iteration population, r and t are individual sequence numbers in the current iteration population, and $r \neq t \neq i$.

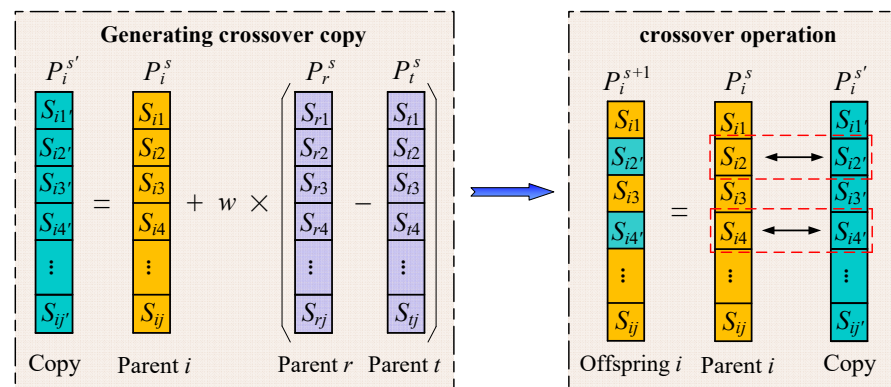


Figure 10. Crossover operator schematic.

In addition, the variable w in the figure represents the scaling factor. In the DE algorithm, w is a constant, which is not conducive to the iterative optimization of the algorithm. In the early stages of algorithm optimization, to avoid the population falling into a local optimum, a relatively large scaling factor needs to be used. In the later stages of algorithm optimization, it is necessary to reduce the scaling factor to increase local exploration intensity. Therefore, in the crossover operator of the PAGA-DE algorithm,

starting from the cosine law, the scaling factor w is designed as a dynamically changing function with the iteration count. It is represented as

$$w = \begin{cases} \frac{1 + \{\cos[(Iter-1)\pi / (Iter_{max}-1)]\}^k}{2}, & (i \leq \frac{i_{max}}{2}) \\ \frac{1 - |\cos[(Iter-1)\pi / (Iter_{max}-1)]|^k}{2}, & (i > \frac{i_{max}}{2}) \end{cases} \quad (51)$$

where $Iter$ indicates the current iteration times, $Iter_{max}$ indicates the maximum number of iterations, and k is the decreasing exponent, $0 < k \leq 1$.

The solution steps of PAGA-DE algorithm are shown in Figure 11.

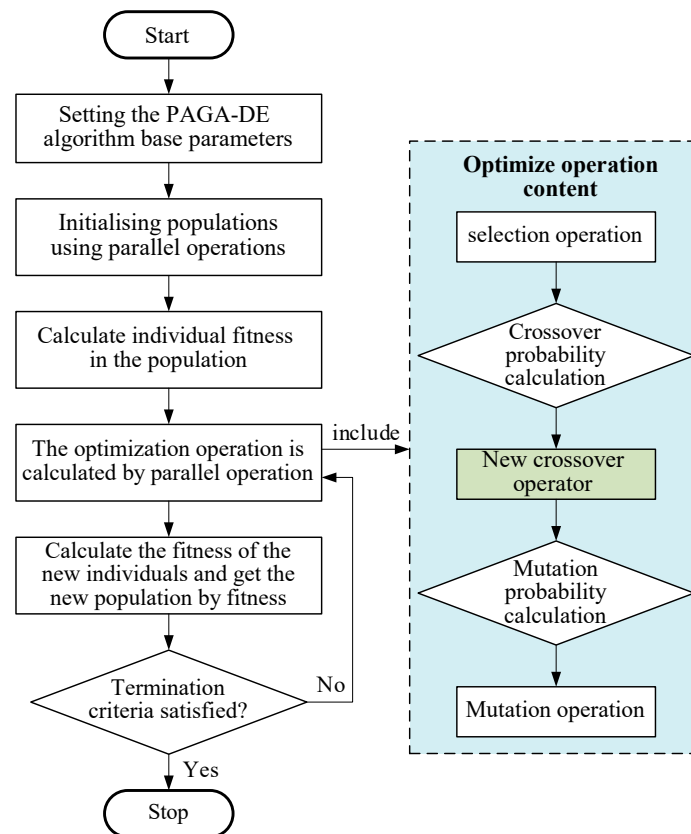


Figure 11. The flowchart of PAGA-DE algorithm.

4. Results and Discussion

To validate the proposed multi-objective optimization design method for the cycloid-pin gear, an analysis is conducted based on the optimization results from three aspects: backlash, transmission error, and torsional stiffness. Therefore, the design variables before and after optimization are separately incorporated into the mathematical models for backlash and transmission error in Sections 2.1 and 2.2, and Monte Carlo simulation is employed for the analysis. Since the design variables are parameters within the cycloid-pin gear, the torsional stiffness is analyzed from two aspects: the equivalent torsional stiffness model of the cycloid-pin gear in Section 2.3.2 and the stiffness of the turning arm bearing in Section 2.3.3. It is noted that, according to Equation (37), the stiffness of the output arm bearing is primarily related to the radial force it experiences. Therefore, the analysis of the bearing force is incorporated into the results.

The RV-80E reducer is taken as an optimization example. Table 3 presents the operating conditions and partial basic parameters of the reducer, while also including the configuration of the PAGA-DE algorithm. Tables 4 and 5 are the error parameters that do not participate in optimization in the backlash and transmission error, respectively.

Table 3. Setting of basic parameters.

	Parameter	Numerical Value
Operating conditions and partial basic parameters of the RV reducer	Input speed n_1	1215 r/min
	Input power P	1.64 kW
	Load torque T	784 N·m
	Transmission ratio i_z	81
	Number of teeth of the sun gear z_1	21
	Number of teeth of the planet gear z_2	42
	Module m	1.5
	Number of cycloid gear teeth z_c	39
	Number of pins z_p	40
PAGA-DE algorithm	Population size M	50
	Maximum crossover probability P_{c1}	1
	Minimum crossover probability P_{c2}	0.7
	Maximum mutation probability P_{m1}	0.1
	Minimum mutation probability P_{m2}	0.05

Table 4. The value of the error parameter in the backlash (Unit: μm).

Error Parameter	Upward Deviation	Lower Deviation	Tolerance
E_w	−25	−45	20
ΔF_α	15	−15	30
ΔF_r	14	0	14
δt	10	−10	20
δa	3	0	3
$\delta \Delta r_p$	1	−1	2
$\delta \Delta R_p$	1.2	−1.2	2.4
Δu	4	1	3

Table 5. The value of the error parameter in the transmission error (Unit: μm).

Error Parameter	Upward Deviation	Lower Deviation	Tolerance
E_s	10	0	10
E_p	12	0	12
A_s	10	0	10
δR_a	5	−5	10
δ_H	5	−5	10
δC_h	5	0	5
δC_s	3	0	3
δP_q	5	0	5
δP_a	5	0	5

4.1. Comparison of Optimization Algorithms

The PAGA-DE and GA algorithms are applied to solve the multi-objective model in this study. In order to verify that the PAGA-DE algorithm has higher computational efficiency and convergence than the GA algorithm, this paper will be divided into two parts: simulated optimization solution and complete optimization solution.

Initially, the maximum number of iterations $Iter_{max}$ is set to 20 in the simulation optimization solution, and 3 calculations are performed, obtaining the runtimes as shown in Table 6. The computer hardware is an AMD Ryzen 9 5900X 12-Core Processor and 128 GB RAM. The average runtime for the PAGA-DE algorithm is 4755 s, while for the GA algorithm, it is 13,941 s. It is evident that, compared to the GA algorithm, the PAGA-DE algorithm improves optimization efficiency by more than 65.89%.

Table 6. Run time comparison.

Optimization Algorithm	Serial Number	Time (s)
GA	1	14,701
	2	13,813
	3	13,308
PAGA-DE	1	4787
	2	4740
	3	4739

Additionally, in the complete optimization solution, by setting the maximum number of iterations $Iter_{max}$ to 100 for optimization, convergence curves for different algorithms are obtained, as shown in Figure 12. In the figure, at the end of the first iteration, the fitness value of the PAGA-DE algorithm is significantly higher than that of the GA algorithm. Moreover, the convergence curve of the PAGA-DE algorithm is approaching stability by the 15th iteration cycle, while the GA algorithm achieves a stable convergence curve only around the 69th iteration cycle. The results indicate a significant improvement in both convergence and computational efficiency for the improved PAGA-DE algorithm. The optimized data is solved using the PAGA-DE algorithm, filled in Table 7, and rounded. In the optimized data, the unrounded design variables are placed in (), as shown in Table 7(a,b).

Table 7. Before and after optimization data.

(a) Geometric dimensions and modifications						
Parameter	Before optimization			After optimization		
R_p (mm)	75			77.4 (77.37)		
r_p (mm)	3.5			3.8 (3.81)		
a (mm)	1.5			1.6 (1.59)		
b (mm)	10			14.7 (14.71)		
Δr_p (μm)	−15			−7 (−7.18)		
ΔR_p (μm)	−30			−13 (−12.73)		
(b) Dimensional accuracy (Unit: μm)						
Error parameter	Before optimization			After optimization		
	Upward deviation	Lower deviation	Tolerance	Upward deviation	Lower deviation	Tolerance
$\delta R_p(T_{\delta R_p})$	2	−8	10	3	−9	12 (12)
$\delta r_p(T_{\delta r_p})$	−1.5	−4.5	3	−1	−5	4 (4.15)
$\delta F_{r1}(T_{\delta F_r})$	10	0	10	7	0	7 (6.77)
$\delta F_p(T_{\delta F_p})$	10	0	10	8	0	8 (7.95)
(c) Objective function						
Objective function	Before optimization			After optimization		
Backlash characterization coefficient	0.86			0.91		
Mean value of transmission error (")	36.03			34.17		
Torsion angle (")	105.2			95.84		

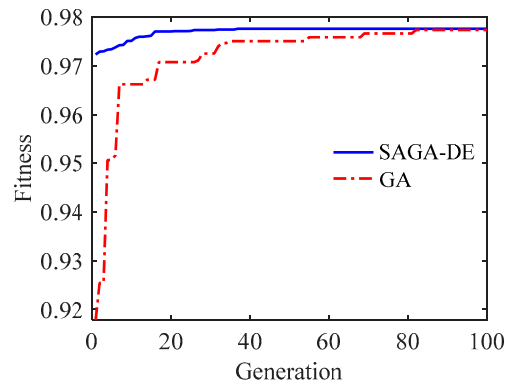


Figure 12. Convergence diagram of the algorithm.

4.2. Analysis of Backlash before and after Optimization

According to the design variables before and after optimization, the Monte Carlo method was used to calculate the backlash of RV reducers. The results of the backlash before and after optimization are entered in Table 8 and fitted to the curve as shown in Figure 13. As can be seen from the curve in the figure, the backlash has a normal distribution trend. Before optimization, the range of backlash is between 0.53' and 2.06', with a mean of 1.23'. The number of simulation experiments with deviations within 1.5' was 18,318, accounting for 91.75%. After optimization, the range of backlash is between 0.05' and 1.61', with a mean of 0.81'. The number of simulation experiments with deviations within 1.5' is 19,998, accounting for 99.99%. Based on the comparison of backlash before and after optimization, it is concluded that the maximum value of backlash after optimization has decreased by 21.84%, and the reliability of backlash accuracy has improved by 8.24%.

Table 8. Number and percentage of the backlash with 1.5' before and after optimization.

	Number of the Backlash within 1.5'	Proportion
Before optimization	18,318	91.75%
After optimization	19,998	99.99%

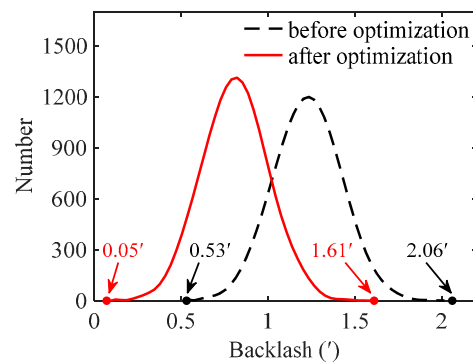


Figure 13. Backlash before and after optimization.

4.3. Analysis of Transmission Error before and after Optimization

As above, the Monte Carlo method is used to calculate the transmission error of RV reducers. Before and after the optimization, the sample data from the Monte Carlo experiments is entered in Table 9 and fitted to the curve as shown in Figure 14. The distribution curve of the transmission error value tends to be Rayleigh-distributed. Before optimization, the maximum value of transmission error can be 93.43'', the mean value is 36.03'', and there are 19,433 times within 60'', accounting for 97.17%. After optimization, the maximum value of transmission error can be 88.68'', the mean value is 34.17'', and there are 19,704 times within 60'', which is 98.52% of the time. Based on the comparison

of the numerical results of the transmission error before and after the optimization, the maximum value of the transmission error is reduced by 5.08% after the optimization, the mean value is reduced by 5.16%, and the number of times it is within 1' is improved by 1.35% compared to that before the optimization.

Table 9. Number and percentage of transmission error with 1.5' before and after optimization.

	Number of Transmission Error within 60''	Proportion
Before optimization	19,433	97.17%
After optimization	19,704	98.52%

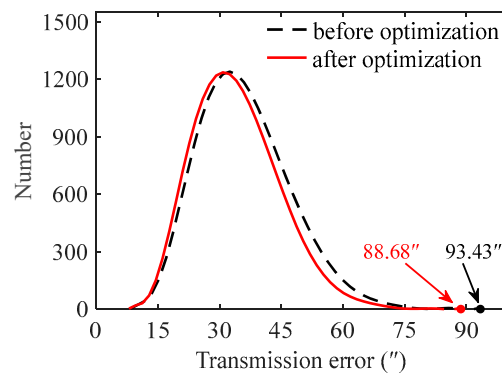


Figure 14. Transmission error before and after optimization.

4.4. Analysis of Torsional Stiffness before and after Optimization

As can be seen from Table 7, before and after optimization data, the torsion angle at the output end of RV machine before optimization is 105.2'', and the torsion angle after optimization is 95.84'', which is reduced by 8.9%. This reflects that the torsional rigidity of the RV is improved after optimization, and the transmission accuracy of RV reducers is improved when the load is driven.

Based on the equivalent torsional stiffness model of the cycloid pinwheel in Section 2.3.2, the changes in the equivalent torsional stiffness of the cycloid pinwheel pair before and after optimization are obtained (Figure 15), and the equivalent torsional stiffness of each pair of teeth is filled in Table 10. From the data in Figure 15 and Table 10, it can be seen that the phase angle interval of the meshing tooth pair before optimization is 18°~72°, with 7 pairs of teeth participating in engagement. The equivalent torsional stiffness for each pair of engaging teeth ranges from $4.26 \times 10^8 \sim 6.1 \times 10^9$ N·mm/rad, and the total equivalent torsional stiffness is 3×10^{10} N·mm/rad. The phase angles of the optimized meshing pairs of teeth ranged from 18° to 72°, with seven pairs of teeth engaged. The equivalent torsional stiffness of each pair of meshing teeth ranged from $7.7 \times 10^8 \sim 1.02 \times 10^{10}$ N·mm/rad, with a total equivalent torsional stiffness of 5.01×10^{10} N·mm/rad. The number of meshed tooth pairs remains the same after optimization, but the total equivalent torsional stiffness is increased by 67.39% compared to the pre-optimization. Consequently, the load-bearing capacity of the cycloid-pin gear mechanism is improved.

Table 10. The equivalent torsional stiffness before and after optimization.

	The Equivalent Torsional Stiffness $\times 10^9$ (N·mm/rad)							Summation
	1	2	3	4	5	6	7	
Before optimization	0.426	1.69	6.08	5.98	5.69	5.29	4.8	29.96
After optimization	0.773	3.46	10.17	9.89	8.37	8.66	7.85	50.15

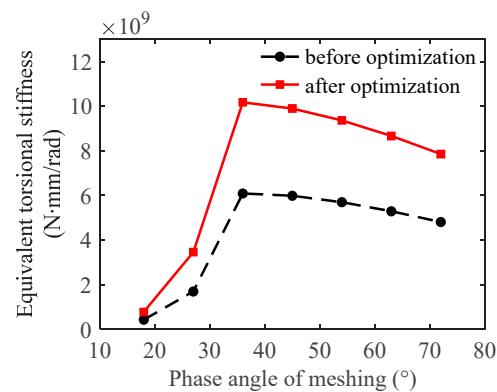


Figure 15. Equivalent torsional stiffness before and after optimization of the cycloid-pin gear pair.

To further analyze the change in torsional stiffness, based on the calculation model for the torsional angle of the arm-bearing in Section 2.3.3, the variation in radial force on the turning arm bearing with the crankshaft angle before and after optimization is obtained (Figure 16). The maximum radial force on the turning arm bearing before optimization is 5173.1 N, and after optimization, it is reduced to 5039 N, a decrease of 2.59%. The reduction in the maximum force on the bearing indicates a decrease in the contact stress between the cylindrical rollers of the turning arm bearing and the inner and outer rings. This situation is beneficial for improving the service life of the turning arm bearing.

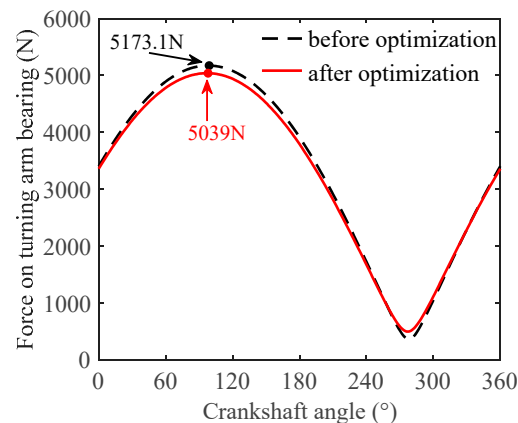


Figure 16. Forces on turning arm bearings before and after optimization.

5. Conclusions

In this work, a multi-objective optimization model used in the manufacturing and processing parameters of the cycloid-pin gear in RV reducers has been proposed. The model is optimized for backlash, transmission error, and torsional stiffness.

- (1) With the backlash, transmission error, and torsion angle as the optimization objectives, the geometric parameters, dimensional accuracy, and modification amount of cycloid-pin gear pairs as the design variables, the multi-objective optimization model is established from the constraints of geometric parameters and the requirements of design criteria.
- (2) Based on the AGA algorithm and DE algorithm, an improved PAGA-DE algorithm is proposed. By comparing with the GA algorithm, it is concluded that the PAGA-DE algorithm has improved its solving efficiency and optimization ability, which proves that the computational efficiency and convergence accuracy of the PAGA-DE algorithm to solve the optimization model basically achieve the expected effect.
- (3) After optimization, the proportion of backlash within 1.5' is 99.99%, and the reliability of return difference is increased by 8.24%. Transmission error within 60'' accounted

for 98.52%, an increase of 1.35%. The torsion angle of the whole machine is reduced to 95.84'', which is reduced by 8.9% compared with before optimization. The driving performance and service life of RV reducers are improved. The design guidance of the macro and micro angle of the transmission system is realized. It lays a theoretical foundation for the engineering practice of precision transmission. By comparing the data of the three major performance indexes before and after optimization, the established optimization model achieves the improvement of the transmission performance of the reducer after solving, which is in line with the expected goal.

This paper has essentially achieved error control in the transmission system and provided design guidance for geometric dimensions. Moreover, the established optimization model and proposed improvement algorithm offer theoretical support for research in the optimization of reducers, providing a solid foundation for further studies.

First of all, according to the mathematical model of manufacturing and processing parameters and transmission performance established in this paper, the parameters of the cycloid-pin gear pair, the involute gear system, and the planetary carrier can be further optimized. This will enable a more comprehensive optimization design, providing more precise data support.

Secondly, on the basis of the research in this paper, more optimization objectives can be considered to establish a more comprehensive optimization model. For instance, transmission efficiency, originally treated as a constraint, can be transformed into an optimization objective. This transformation enables optimization design considering complex operating conditions such as transmission accuracy, load-bearing performance, and energy utilization efficiency. The use of a quality loss function in this paper to characterize the processing cost of dimensional accuracy may not precisely calculate actual processing costs. Therefore, introducing a processing cost function on the basis of this paper can optimize design with considerations for both cost and performance requirements.

Certainly, as the number of objective functions and design variables increases, further research is needed on how to more effectively solve the optimization model. The improved PAGA-DE algorithm in this paper makes a contribution to such research.

Author Contributions: Conceptualization, Y.Z.; methodology, Y.Z., Z.H. and Q.T.; validation, Y.Z., Z.H. and W.S.; formal analysis, Q.T. and W.S.; investigation, Y.Z.; data curation, H.W.; writing—original draft preparation, Y.Z.; writing—review and editing, Z.H., Q.T. and R.L.; supervision, Y.D.; project administration, Z.H. All authors have read and agreed to the published version of the manuscript.

Funding: This research was funded by National Natural Science Foundation of China (No. 52005229), Natural Science Foundation of Jiangsu (No. BK20201055), Sponsored by Qing Lan Project of Jiangsu (No. KYQ20004), Leading Innovative Talent Introduction and Cultivation Program of Changzhou (No. CQ20210119&CQ20230075), and Graduate Practice Innovation Program of Jiangsu University of Technology (No. XSJXC22_45).

Data Availability Statement: Data are contained within the article.

Acknowledgments: The authors wish to extend their sincere appreciation to their advisor, Han Zhenhua, for his guidance, and the reviewers who provided related suggestions and recommendations for this manuscript.

Conflicts of Interest: The authors declare no conflicts of interest.

References

1. Pham, A.D.; Ahn, H.J. High Precision Reducers for Industrial Robots Driving 4th Industrial Revolution: State of Arts, Analysis, Design, Performance Evaluation and Perspective. *Int. J. Precis. Eng. Manuf.-Green Technol.* **2018**, *5*, 519–533. [[CrossRef](#)]
2. Yang, M.D.; Zhang, D.Q.; Cheng, C.; Xu, H. Reliability-based design optimization for RV reducer with experimental constraint. *Struct. Multidiscip. Optim.* **2021**, *63*, 2047–2064. [[CrossRef](#)]
3. Zhang, T.; Li, X.; Wang, Y.W.; Sun, L.N. A semi-analytical load distribution model for cycloid drives with tooth profile and longitudinal modification. *Appl. Sci.* **2020**, *10*, 4859. [[CrossRef](#)]

4. Huang, J.; Li, C.Y.; Zhang, Y.; Wang, Y.H.; Chen, B.K. Transmission error analysis of cycloidal pinwheel meshing pair based on rolling-sliding contact. *J. Braz. Soc. Mech. Sci.* **2021**, *43*, 355. [[CrossRef](#)]
5. Li, X.; Huang, J.Q.; Ding, C.C.; Guo, R.; Niu, W.L. Dynamic Modeling and Analysis of an RV Reducer Considering Tooth Profile Modifications and Errors. *Machines* **2023**, *11*, 626. [[CrossRef](#)]
6. Fiorineschi, L.; Frillici, F.S.; Pugi, L.; Rotini, F. Impact of Cycloid's and Roller's Dimensional Errors on the Performance of a Cycloidal Drive for Power Transmission. *Machines* **2023**, *11*, 772. [[CrossRef](#)]
7. Li, Y.H.; Li, W.; He, W.D. RV reducer backlash analysis based on robust design. *Appl. Mech. Mater.* **2012**, *148*, 418–421. [[CrossRef](#)]
8. Han, L.S.; Guo, F. Global sensitivity analysis of transmission accuracy for RV-type cycloid-pin drive. *J. Mech. Sci. Technol.* **2016**, *30*, 1225–1231. [[CrossRef](#)]
9. Li, T.X.; Wang, G.F.; Deng, X.Z.; An, X.T.; Xing, C.R.; Ma, W.S. Contact Analysis of Cycloidal-pin Gear of RV Reducer Under the Influence of Profile Error. *J. Phys. Conf. Ser.* **2019**, *1168*, 022095. [[CrossRef](#)]
10. Ahn, H.J.; Choi, B.M.; Lee, Y.H.; Pham, A.D. Impact analysis of tolerance and contact friction on a RV reducer using FE method. *Int. J. Precis. Eng. Manuf.* **2021**, *22*, 1285–1292. [[CrossRef](#)]
11. Sun, Y.G.; Zhao, X.F.; Jiang, F.; Zha, L.; Liu, D.; Yu, G.B. Backlash analysis of RV reducer based on error factor sensitivity and Monte-Carlo simulation. *Int. J. Hybrid Inf. Technol.* **2014**, *7*, 283–292. [[CrossRef](#)]
12. Zhao, H.M.; Wang, M.; Zhang, L.L.; Li, H.W.; Zhang, H.L. Static Backlash Analysis and Study on Error Distribution of RV Reducer. *J. Tianjin Univ. (Sci. Technol.)* **2016**, *49*, 164–170.
13. Chu, X.Y.; Xu, H.H.; Wu, X.M.; Tao, J.P.; Shao, G.F. The method of selective assembly for the RV reducer based on genetic algorithm. *Proc. Inst. Mech. Eng. Part C J. Mech. Eng. Sci.* **2018**, *232*, 921–929. [[CrossRef](#)]
14. Lin, K.S.; Chan, K.Y.; Lee, J.J. Kinematic error analysis and tolerance allocation of cycloidal gear reducers. *Mech. Mach. Theory* **2018**, *124*, 73–91. [[CrossRef](#)]
15. Lin, W.S.; Shih, Y.P.; Lee, J.J. Design of a two-stage cycloidal gear reducer with tooth modifications. *Mech. Mach. Theory* **2014**, *79*, 184–197. [[CrossRef](#)]
16. Lu, L.S.; Zhang, F.X.; Wan, Z.P.; Tang, Y. Cycloidal Gear Tooth Profile Modification of RV Reducer Based on Backlash Optimization. *J. South China Univ. Technol. (Nat. Sci. Ed.)* **2018**, *46*, 1–8.
17. Sun, X.X.; Han, L.; Wang, J. Tooth modification and loaded tooth contact analysis of China Bearing Reducer. *Proc. Inst. Mech. Eng. Part C J. Mech. Eng. Sci.* **2019**, *233*, 6240–6261. [[CrossRef](#)]
18. Brumerick, F.; Lukac, M.; Caban, J.; Krzysiak, Z.; Glowacz, A. Comparison of Selected Parameters of a Planetary Gearbox with Involute and Convex-Concave Teeth Flank Profiles. *Appl. Sci.* **2020**, *10*, 1417. [[CrossRef](#)]
19. Figlus, T.; Koziol, M.; Kuczyński, Ł. Impact of Application of Selected Composite Materials on the Weight and Vibroactivity of the Upper Gearbox Housing. *Materials* **2019**, *12*, 2517. [[CrossRef](#)]
20. Brumerick, F.; Tomasikova, M.; Nieoczym, A. Epicyclic Gear Train Synthesis. *Commun.-Sci. Lett. Univ. Zilina* **2015**, *17*, 47–50. [[CrossRef](#)]
21. Blagojevic, M.; Marjanovic, N.; Djordjevic, Z.; Stojanovic, B.; Marjanovic, V.; Vujanac, R.; Disic, A. Numerical and experimental analysis of the cycloid disc stress state. *Teh. Vjesn.* **2014**, *21*, 377–382.
22. Li, T.X.; Tian, M.; Xu, H.; Deng, X.Z.; An, X.T.; Su, J.X. Meshing contact analysis of cycloidal-pin gear in RV reducer considering the influence of manufacturing error. *J. Braz. Soc. Mech. Sci.* **2020**, *42*, 1–14. [[CrossRef](#)]
23. Qiao, X.T.; Zhang, L.B.; Chen, C.S.; Yan, C.F.; Wang, C.L.; Wang, W.G. Study on transient contact performance of meshing transmission of cycloid gear and needle wheel in RV reducer. *J. Eng.* **2020**, *14*, 1001–1004.
24. Li, T.X.; Xu, H.; Tian, M. A Loaded Analysis Method for RV Cycloidal-pin Transmission Based on the Minimum Energy Principle. *Stroj. Vestn.-J. Mech. Eng.* **2020**, *66*, 655–667. [[CrossRef](#)]
25. Li, X.; Tang, L.; He, H.; Sun, L. Design and Load Distribution Analysis of the Mismatched Cycloid-Pin Gear Pair in RV Speed Reducers. *Machines* **2022**, *10*, 672. [[CrossRef](#)]
26. Bednarczyk, S.; Jankowski, L.; Krawczyk, J. The influence of eccentricity changes on power losses in cycloidal gearing. *Tribologia* **2019**, *285*, 19–29. [[CrossRef](#)]
27. Xu, L.X.; Chen, B.K.; Li, C.Y. Dynamic modelling and contact analysis of bearing-cycloid-pinwheel transmission mechanisms used in joint rotate vector reducers. *Mech. Mach. Theory* **2019**, *137*, 432–458. [[CrossRef](#)]
28. Zhang, Y.M.; Li, L.S.; Ji, S.T. Influence of cycloid-pin gear design parameters on bearing capacity and optimized design. *J. Braz. Soc. Mech. Sci.* **2022**, *4*, 123. [[CrossRef](#)]
29. Li, X.; Chen, B.K.; Wang, Y.W.; Lim, T.C. Mesh stiffness calculation of cycloid-pin gear pair with tooth profile modification and eccentricity error. *J. Cent. South Univ.* **2018**, *25*, 1717–1731. [[CrossRef](#)]
30. Wang, J.; Luo, S.M.; Su, D.Y. Multi-objective optimal design of cycloid speed reducer based on genetic algorithm. *Mech. Mach. Theory* **2016**, *102*, 135–148. [[CrossRef](#)]
31. Wang, Y.L.; Qian, Q.J.; Chen, G.D.; Jin, S.S.; Chen, Y. Multi-objective optimization design of cycloid pin gear planetary reducer. *Adv. Mech. Eng.* **2017**, *9*, 1–10. [[CrossRef](#)]
32. Zhang, Y.; Huang, J.Y.; He, W. Multi-objective optimization of cycloidal gear based on segmental modification of pressure angle. *J. Mech. Sci. Technol.* **2022**, *36*, 3535–3545. [[CrossRef](#)]
33. Wu, S.Z.; He, W.D.; Zhang, Y.H. Multi-objective optimization design of RV planetary transmission system with small tooth difference. *Acad. J. Manuf. Eng.* **2018**, *16*, 98–106.

34. Song, X.P.; Chen, Y.; Yang, J.M. Study of the transmission characteristics of the cycloid gear based on a multi-objective optimization modification. *Machines* **2023**, *11*, 775. [[CrossRef](#)]
35. Rai, P.; Agrawal, A.; Saini, M.L.; Jodder, C.; Barman, A.G. Volume optimization of helical gear with profile shift using real coded genetic algorithm. *Procedia Comput. Sci.* **2018**, *133*, 718–724. [[CrossRef](#)]
36. Daoudi, K.; Boudi, E.M.; Abdellah, M. Genetic Approach for Multiobjective Optimization of Epicyclic Gear Train. *Math. Probl. Eng.* **2019**, *2019*, 9324903.
37. Yao, Q.Z. Multi-objective optimization design of spur gear based on NSGA-II and decision making. *Adv. Mech. Eng.* **2019**, *11*, 1–8. [[CrossRef](#)]
38. Cui, Z.Y.; Song, C.S.; Zhu, F.H.; Zhu, C.C. Research on Tolerance Design of 2K-V Reducer with Beveloid Gear Considering the Effect of Anti-Backlash. *Int. J. Precis. Eng. Manuf.* **2023**, 1–14. [[CrossRef](#)]
39. Wang, Y.K.; Zheng, J.Y.; Chen, T.Q.; Li, L.X. The Analysis Research of the Geometric Lost Motion of High Accurate RV Reducer Used in Robot. *J. Dalian Inst. Railw. Technol.* **1999**, *20*, 24–27.
40. Yang, Y.H.; Zhou, G.C.; Chang, L.; Chen, G. A modelling approach for kinematic equivalent mechanism and rotational transmission error of RV reducer. *Mech. Mach. Theory* **2021**, *163*, 104384. [[CrossRef](#)]
41. Hidaka, T.; Wang, H.Y.; Ishida, T.; Matsumoto, K.; Hashimoto, M. Rotational Transmission Error of K-H-V Planetary Gears With Cycloid Gear: 1st Report, Analytical Method of the Rotational Transmission Error. *Trans. Jpn. Soc. Mech. Eng. C* **1994**, *60*, 645–653. [[CrossRef](#)]
42. Han, L.S.; Shen, Y.W.; Dong, H.J.; Wang, G.F.; Liu, J.Y.; Qi, H.J. Theoretical research on dynamic transmission accuracy for 2K-V-type drive. *Chin. J. Mech. Eng.* **2007**, *43*, 81–86. [[CrossRef](#)]
43. Zhang, Z.; Zhang, G.R.; Zhang, H.W. *Practical Gear Design and Calculation*; China Machine Press: Beijing, China, 2011.
44. ISO 6336-3:2019; Calculation of Load Capacity of Spur and Helical Gears—Part 3: Calculation of Tooth Bending Strength. International Organization for Standardization: Geneva, Switzerland, 2006; Volume 6336, p. 1996.
45. Zhao, Z.H.; Zhang, Q. Study of contact load on cycloid wheel of RV reducer based on MATLAB. In Proceedings of the 2022 8th International Conference on Mechanical Engineering, Materials and Automation Technology (MMEAT 2022), Qingdao, China, 27–29 May 2022.
46. Liu, J.Y.; Matsumura, S.; Chen, B.K.; Houjoh, H. Torsional stiffness calculation of double-enveloping cycloid drive. *J. Adv. Mech. Des. Syst. Manuf.* **2012**, *6*, 2–14. [[CrossRef](#)]
47. Yang, Y.H.; Zhu, L.Y.; Chen, Z.Y.; Shen, Z.G. Analysis of the Characteristics of Torsional Stiffness of RV Reducer. *J. Tianjin Univ. (Sci. Technol.)* **2015**, *48*, 111–118.
48. Wang, G.; Guo, M.L. Stiffness of aerospace rolling bearings. *J. Harbin Inst. Technol.* **2001**, *10*, 644–645+650.
49. Chen, S.T.; Su, W.H. Tolerance optimization design of RV reducer's cycloid-pin gear pair considering multiple targets. In Proceedings of the International Conference on Optical Technology, Semiconductor Materials, and Devices (OTSMD 2022), Xiamen, China, 28–30 October 2022.
50. Kwon, S.M.; Kim, C.H.; Shin, J.H. Optimal rotor wear design in hypotrochoidal gear pump using genetic algorithm. *J. Cent. South Univ.* **2011**, *18*, 718–725. [[CrossRef](#)]
51. Pourmostaghimi, V.; Heidari, F.; Khalilpourazary, S.; Qazani, M.R.C. Application of Evolutionary Optimization Techniques in Reverse Engineering of Helical Gears: An Applied Study. *Axioms* **2023**, *12*, 252. [[CrossRef](#)]
52. Abderazek, H.; Yildiz, A.R.; Sait, S.M. Mechanical engineering design optimisation using novel adaptive differential evolution algorithm. *Int. J. Veh. Des.* **2019**, *80*, 285–329. [[CrossRef](#)]
53. Wang, Y.W.; Filippini, M.; Bacco, G.; Bianchi, N. Parametric design and optimization of magnetic gears with differential evolution method. *IEEE Trans. Ind. Appl.* **2019**, *55*, 3445–3452. [[CrossRef](#)]
54. Herrera, F.; Lozano, M. Fuzzy adaptive genetic algorithms: Design, taxonomy, and future directions. *Soft Comput.* **2003**, *7*, 545–562. [[CrossRef](#)]
55. Mokshin, A.V.; Mokshin, V.V.; Sharnin, L.M. Adaptive genetic algorithms used to analyze behavior of complex system. *Commun. Nonlinear Sci.* **2019**, *71*, 174–186. [[CrossRef](#)]
56. Acebron, J.A.; Herrero, J.R.; Monteiro, J. A highly parallel algorithm for computing the action of a matrix exponential on a vector based on a multilevel Monte Carlo method. *Comput. Math. Appl.* **2020**, *79*, 3495–3515. [[CrossRef](#)]

Disclaimer/Publisher's Note: The statements, opinions and data contained in all publications are solely those of the individual author(s) and contributor(s) and not of MDPI and/or the editor(s). MDPI and/or the editor(s) disclaim responsibility for any injury to people or property resulting from any ideas, methods, instructions or products referred to in the content.